Breakup mechanisms in heavy-ion collisions at low energies

L. Shvedov,[1] M. Colonna,[1,*] and M. Di Toro[1,2]
[1]*Laboratori Nazionali del Sud, INFN, via S. Sofia 62, I-95123 Catania, Italy*
[2]*Physics and Astronomy Department, University of Catania, Catania, Italy*
(Received 9 March 2009; published 18 May 2010)

We investigate reaction mechanisms occurring in heavy-ion collisions at low energy (∼20 MeV/nucleon). In particular, we focus on the competition between fusion and breakup processes (deep inelastic and fragmentation) in semiperipheral collisions, where the formation of excited systems under various conditions of shape and angular momentum is observed. Adopting a Langevin treatment for the dynamical evolution of the system configuration, described in terms of shape observables such as quadrupole and octupole moments, we derive fusion and fission probabilities, from which the corresponding fusion and breakup cross sections can finally be evaluated. The dependence of the results on shape, angular momentum, and excitation energy is discussed.

DOI: 10.1103/PhysRevC.81.054605 PACS number(s): 25.70.Lm, 21.30.Fe, 24.60.Ky, 25.70.Jj

I. INTRODUCTION

Nuclear reactions between medium-mass nuclei at low energies (∼20 MeV/nucleon) offer the possibility to investigate several aspects of dissipative mean-field dynamics and to probe nuclear matter under extreme conditions with respect to shape, spin, and excitation energy. In this energy domain, well above the Coulomb barrier but below the Fermi energies, one essentially observes two types of reaction mechanisms: Fusion dominates in the case of central and semiperipheral collisions, while binary reseparation processes, associated with deep-inelastic or fast-fission mechanisms, essentially involve the remaining range of (semi)peripheral reactions [1]. However, along the transition from fusion to binary processes, composite systems with a rather elongated shape and large intrinsic angular momentum can be formed, corresponding to metastable (or even unstable) conditions, where mean-field fluctuations may play a decisive role in determining the final outcome. The presence of large event-by-event variances related to the onset of new instabilities has already been noted in experiments, from the anomalous distribution of primary fragment properties in binary events [2,3]. The observed variances (in mass, charge, excitation energy, angular distribution) appeared to be much larger than those predicted by mean-field nucleon exchange models. Similar conclusions were reached in theory simulations based on stochastic transport models [4].

Interaction times are quite long and a large coupling among various mean-field modes is expected, leading to the coexistence of different reaction mechanisms in semicentral collisions. Study of the competition between fusionlike and binarylike processes—and, more generally, of the fate of the hot nuclear residues created in these reactions—is a longstanding problem, from which a lot about mean-field dynamics and fundamental properties of nuclear forces can be learned. This issue has recently received renewed interest, owing to the possibility of performing new analyses involving neutron-rich or even exotic systems [5]. Under these conditions the reaction mechanism characterizing dissipative collisions is expected to be sensitive to the density dependence of the isovector part of the nuclear interaction, a matter that is largely debated nowadays [5,6].

In reactions involving medium-heavy nuclei, as a result of the complex neck dynamics, one can also observe, in sufficiently inelastic collisions, new modes of reseparation of the colliding system, such as dynamical ternary breaking, with massive fragments nearly aligned along a common separation axis [7,8]. Experimental evidence of this mechanism has recently been reported in the case of ^{197}Au + ^{197}Au collisions at 15 MeV/nucleon, where aligned quaternary breaking has also been observed [9]. These effects could still be explained in terms of the persistence of the excitation of shape and rotational modes in projectile-like fragments (PLFs) and/or targetlike fragments (TLFs) that are formed in binarylike events, which would lead to further reseparation along a preferential axis, similar to what happens in fast-fission processes of PLFs or TLFs. It is worth mentioning that, at a higher beam energy (∼40 MeV/nucleon), where, apart from mean-field effects, two-body correlations are important, ternary breakings become the dominant process, and new features are observed, corresponding to the emission of small fragments coming directly from the strongly interacting neck region [10]. Actually one may think in terms of a smooth transition between the different decay modes of PLFs and/or TLFs from fast fission, characterized by splitting into fragments of similar size and low relative velocity, to neck emission, where small fragments are emitted at a higher relative velocity with respect to PLFs and TLFs.

From the preceding discussion, it is clear that understanding the competition between reaction mechanisms in dissipative collisions, as well as the nature of new exotic reseparation modes, requires a thorough analysis of the underlying mean-field dynamics and associated shape fluctuations and rotational effects. In this paper, we attempt to improve the dynamical description of low-energy collisions by coupling a microscopic transport approach based on mean-field concepts, suitable for following the early stage of the collision up to the formation of composite excited sources, to a more refined treatment of the dynamics of shape observables, including the associated fluctuations within the Langevin scheme [11], for the following

*colonna@lns.infn.it

evolution up to the definition of the final outcome. In particular, we discuss the dynamics of excited sources characterized by given values of quadrupole and octupole moments and intrinsic angular momentum. This allows one to investigate the competition between fusionlike and binarylike reaction mechanisms and to evaluate fusion cross sections, as well as the probability and the features of fast-fission processes of PLFs (or TLFs). The paper is organized as follows. In Sec. II we present the hybrid transport treatment employed to follow the dynamical evolution of the system. Results concerning the competition between fusion and binary processes are discussed in Sec. III. Finally, conclusions and perspectives are drawn in Sec. IV.

II. SIMULATION OF THE COLLISIONAL DYNAMICS

A. Dynamical description of nuclear reactions

The evolution of systems governed by a complex phase space can be described by a transport equation, of the Boltzmann-Nordheim-Vlasov type, with a fluctuating term, the so-called Boltzmann-Langevin equation (BLE) [12,13]:

$$\frac{df}{dt} = \frac{\partial f}{\partial t} + \{f, H\} = I_{\rm coll}[f] + \delta I[f], \tag{1}$$

where $f(\mathbf{r}, \mathbf{p}, t)$ is the one-body distribution function, that is, the semiclassical analog of the Wigner transform of the one-body density matrix, $H(\mathbf{r}, \mathbf{p}, t)$ the mean-field Hamiltonian, $I_{\rm coll}$ the two-body collision term (that accounts for the residual interaction) incorporating the Fermi statistics of the particles, and $\delta I[f]$ the fluctuating part of the collision integral. The nuclear equation of state, directly linked to the mean-field Hamiltonian H, can be written as

$$E/A(\rho, I) = E_s/A(\rho) + C_{\rm sym}(\rho) I^2 + O(I^4), \tag{2}$$

where $I = (N - Z)/A$ is the asymmetry parameter. We adopt a soft isoscalar equation of state, $E_s/A(\rho)$, with compressibility modulus $K = 200$ MeV, which is favored, for example, from flow studies [14]. For the density (ρ) dependence of the symmetry energy $C_{\rm sym}(\rho)$, we consider a linear increase in the potential part of the symmetry energy with density:

$$C_{\rm sym}(\rho) = a \left(\frac{\rho}{\rho_0}\right)^{2/3} + b \left(\frac{\rho}{\rho_0}\right), \tag{3}$$

where ρ_0 is the saturation density, $a = 13.4$ MeV, and $b = 18$ MeV. From the expression of the energy density, Eq. (2), the mean-field potential is directly derived. The free-energy- and angle-dependent nucleon-nucleon cross section is used in the collision integral [15]. Within this approach, the system is described in terms of the one-body distribution function f, but this function may experience a stochastic evolution in response to the action of the fluctuating term $\delta I[f]$.

However, the numerical resolution of the full BLE is not available yet in three dimensions. Approximate treatments of the BLE have been introduced so far (see Refs. [15] and [16]), such as the stochastic mean-field (SMF) model, which consists in the implementation of stochastic density fluctuations only in coordinate space and can be solved numerically using the test particle method [15]. It should be noticed that semiclassical models have been shown to work well for description of the approaching phase of reactions at energies above the Coulomb barrier, leading to the formation of composite excited systems [17–19]. Moreover, the SMF model is particularly appropriate for description of the evolution of the dilute unstable sources that develop in dissipative collisions at Fermi energies (30–100 MeV/nucleon) [20]. In this context, quantal effects can also be incorporated in the dynamics of the unstable collective modes [21,22].

However, here we are essentially interested in semicentral reactions at lower energies where, most likely, the formation of elongated (rather than dilute) systems is observed, and phenomena associated with surface (rather than volume) metastability and/or instability may take place. To improve the treatment of fluctuations suitable for describing the latter scenario, we adopt a hybrid description of the dynamics: We follow the microscopic SMF evolution until the instant in time when local thermal equilibrium is established and one observes the formation of quasistationary elongated systems, with a density close to the normal value. Then, to deal with the following evolution of the system, we move to a more macroscopic model description, where the system is characterized in terms of global observables, for which the full treatment of fluctuations in phase space is numerically affordable, as explained here.

B. Dynamical evolution of shape observables

This section is devoted to the description of the dynamical evolution of excited systems whose leading degrees of freedom are shape observables, while the density remains always close to the normal value, $\rho_0 = 3/4\pi r_0^3$, r_0 being the nuclear radius constant ($r_0 = 1.2$ fm). The configuration of the system under study, having given charge Z and mass A, is described by three global observables (and associated velocities): the quadrupole moment β_2, the octupole moment β_3, and the rotation angle ω. For situations far from a spherical shape, thermal agitation can induce fluctuations that may eventually lead to breakup channels. Hence correct treatment of shape fluctuations is crucial for characterization of the reaction mechanism. For this purpose, we consider the stochastic extension of the Rayleigh-Lagrange equations of motion [23] (the Langevin equation):

$$\frac{\rm d}{{\rm d}t}\frac{\partial L}{\partial \dot{q}_i} + \frac{\partial F}{\partial \dot{q}_i} = \frac{\partial L}{\partial q_i} + F_{\rm fluc}(t), \tag{4}$$

where $q_i (i = 1, 2, 3) = (\omega, \beta_2, \beta_3)$. $L(q_i, \dot{q}_i) = E_{\rm kin}(q_i, \dot{q}_i) + E_{\rm rot}(q_i, \dot{q}_i) - E_{\rm pot}(q_i)$ denotes the Lagrangian of the system, and

$$F(q_i, \dot{q}_i) = \frac{1}{2}\frac{{\rm d}E_{\rm tot}}{{\rm d}t} = \frac{1}{2}\sum_{i,j=2}^{3} R_{ij}\dot{q}_i\dot{q}_j \tag{5}$$

is the Rayleigh dissipation function. $E_{\rm kin}$, $E_{\rm rot}$ and $E_{\rm pot}$ indicate the kinetic, rotational, and potential energy of the system, respectively, and the quantity R_{ij} is the dissipation tensor. The difference with respect to the standard Rayleigh-Lagrange equations is the fluctuation term $F_{\rm fluc}$, which can be interpreted as a rapidly fluctuating stochastic force, in the same spirit of the Brownian motion, similar to the fluctuating term in the

BLE, Eq. (1). We solve numerically the set (4) of coupled equations.

For given values of the quadrupole and octupole moments, the shape of the system is parametrized, in terms of the polar angle θ, as follows:

$$R(\theta) = R_0(\beta_2, \beta_3)\{1 + \beta_1(\beta_2, \beta_3)Y_{10}(\theta) + \beta_2 Y_{20}(\theta) + \beta_3 Y_{30}(\theta)\}, \quad (6)$$

where the functions $Y_{i0}(\theta)$ are spherical harmonics. The parameters β_1 and R_0 are introduced to conserve the position of the center of mass and the total volume V of the system and can be determined from the equations

$$\int dV z = \frac{2\pi}{4}\int_0^\pi R^4(\theta)\sin\theta\cos\theta d\theta = 0, \quad (7)$$

$$\int dV = \frac{2\pi}{3}\int_0^\pi R^3(\theta)\sin\theta d\theta = \frac{4}{3}\pi r_0^3 A, \quad (8)$$

where z denotes the coordinate along the system maximum elongation axis (or symmetry axis). In the following we discuss in detail the derivation of the different terms of the Lagrangian L.

1. Rotational energy

The rotational energy is simply equal to

$$E_{\rm rot} = \tfrac{1}{2} I(\beta_2, \beta_3)\dot{\omega}^2, \quad (9)$$

where

$$I(\beta_2, \beta_3) = \frac{\pi m \rho_0}{5}\int_0^\pi R^5(\theta)\{1 + \cos^2\theta\}\sin\theta\, {\rm d}\theta \quad (10)$$

is the moment of inertia for the whole system, m being the nucleon mass.

2. Kinetic energy

The kinetic energy can be expressed as follows:

$$E_{\rm kin} = \frac{1}{2}\sum_{i,j=2}^{3} M_{ij}(\beta_2, \beta_3)\dot{q}_i\dot{q}_j. \quad (11)$$

To calculate the mass tensor M_{ij}, we adopt the prescriptions of Ref. [24]:

$$M_{i,j} = \tfrac{1}{2}(M'_{i,j} + M'_{j,i}), \quad (12)$$

with

$$M'_{i,j} = 2\pi m\rho_0\int_0^\pi \sum_{l=1}^{L} b_{il} R^{l+2}(\theta)P_l(\cos\theta) \times \left\{\frac{\partial R_0}{\partial\beta_j}S + R_0\left(\frac{\partial\beta_1}{\partial\beta_j}Y_{10} + Y_{j0}\right)\right\}\sin\theta\, {\rm d}\theta. \quad (13)$$

Here P_l are Legendre polynomials and $S(\theta) = R(\theta)/R_0$. In our calculations we have $L = 5$. The coefficients b_{2l} and b_{3l} are obtained by solving the system of equations

$$\sum_{l=1}^{L} A_{kl} b_{ml} = C_{mk}, \qquad k = 1\cdots L, \quad m = 2, 3, \quad (14)$$

with

$$A_{kl} = \int_0^\pi R^{l-1}(\theta)\left\{l P_l(\cos\theta) - \frac{1}{R(\theta)}\frac{\partial R(\theta)}{\partial\theta}\frac{\partial P_l(\cos\theta)}{\partial\theta}\right\} \cdot R^{k-1}(\theta)\left\{k P_k(\cos\theta) - \frac{1}{R(\theta)}\frac{\partial R(\theta)}{\partial\theta}\frac{\partial P_k(\cos\theta)}{\partial\theta}\right\} \times \sin\theta\, {\rm d}\theta, \quad (15)$$

$$C_{mk} = \int_0^\pi R^{k-1}(\theta)\left\{k P_k(\cos\theta) - \frac{1}{R(\theta)}\frac{\partial R(\theta)}{\partial\theta}\frac{\partial P_k(\cos\theta)}{\partial\theta}\right\} \cdot \left\{\frac{\partial R_0}{\partial\beta_m}S + R_0\left(\frac{\partial\beta_1}{\partial\beta_m}Y_{10} + Y_{m0}\right)\right\}\sin\theta\, {\rm d}\theta. \quad (16)$$

3. Potential energy: Nuclear term

Concerning the nuclear part of the potential energy E_n, we discuss essentially the surface contribution, because our system keeps a constant volume over time. We adopt a double volume integral of the Yukawa-plus-exponential folding function [25]:

$$E_n = -\frac{a_s(1 - k_s I^2)}{8\pi^2 {r_0}^2 a^3}\int_V\int_V\left(\frac{\sigma}{a} - 2\right)\frac{e^{-\sigma/a}}{\sigma}\, {\rm d}^3 r\, {\rm d}^3 r', \quad (17)$$

where a_s is the surface-energy constant, k_s is the surface-asymmetry constant, and a is the range of the Yukawa-plus-exponential potential. σ denotes the modulus of the relative distance $\sigma = |r - r'|$. Parameters have been fitted to the ground-state energies and fission barrier heights [26,27]. To reduce the numerical efforts, the integral of Eq. (17) can be transformed into a double surface integral, by using the twofold Gauss divergence theorem. For axially symmetric shapes, one of the azimuthal integrations can be performed trivially [25,28], and the resulting threefold integral is

$$E_n = \frac{a_s(1 - k_s I^2)}{4\pi {r_0}^2}\iiint\left\{2 - \left[\left(\frac{\sigma}{a}\right)^2 + 2\frac{\sigma}{a} + 2\right]e^{-\sigma/a}\right\} \times \frac{P(\theta, \theta', \phi)P(\theta', \theta, -\phi)}{\sigma^4}{\rm d}\theta\, {\rm d}\theta'\, {\rm d}\phi, \quad (18)$$

where the distance σ can be expressed as

$$\sigma = [R^2(\theta) + R^2(\theta') - 2R(\theta)R(\theta') \cdot \{\cos\theta\cos\theta' + \sin\theta\sin\theta'\cos\phi\}]^{1/2}$$

and

$$P(\theta, \theta', \phi) = R(\theta)\sin\theta\{R^2(\theta) - R(\theta)R(\theta') \times [\cos\theta\cos\theta' + \sin\theta\sin\theta'\cos\phi] - R(\theta')\frac{\partial R(\theta)}{\partial\theta}[\sin\theta\cos\theta' - \cos\theta\sin\theta'\cos\phi]\}.$$

4. Potential energy: Coulomb term

The Coulomb part of the potential energy is taken as [29]:

$$E_C = E_C^{\rm sharp} + \Delta E_C^{\rm dif},$$

where $E_C^{\rm sharp}$ is the Coulomb energy corresponding to a sharp charge-density distribution and $\Delta E_C^{\rm dif}$ is a correction caused by the diffuseness.

The sharp-surface part of the Coulomb energy is equal to

$$E_C^{\text{sharp}} = -\frac{\rho_p^2 \pi}{6} \iiint \frac{P(\theta,\theta',\phi)P(\theta',\theta,-\phi)}{\sigma}\, \mathrm{d}\theta\, \mathrm{d}\theta'\, \mathrm{d}\phi, \tag{19}$$

where ρ_p is the charge (proton) density, $\rho_p = (Z/A)\rho_0$. The correction to the Coulomb energy owing to the diffuseness can be expressed as

$$\Delta E_C^{\text{dif}} = {\rho_p}^2 \pi {a_C}^3 \iiint \left\{ 2\frac{\sigma}{a_C} - 5 + \left[\frac{1}{2}\left(\frac{\sigma}{a_C}\right)^2 + 3\frac{\sigma}{a_C} + 5 \right] e^{-\sigma/a_C} \right\} \times \frac{P(\theta,\theta',\phi)P(\theta',\theta,-\phi)}{\sigma^4}\, \mathrm{d}\theta\, \mathrm{d}\theta'\, \mathrm{d}\phi, \tag{20}$$

where a_C is the range parameter of the Yukawa function generating the diffuse charge distribution [28–30].

5. Dissipation function

The one-body dissipation mechanism is evaluated as follows (see Ref. [23] for details):

$$\frac{\mathrm{d}E}{\mathrm{d}t} = m\rho_0 \overline{v} \oint \dot{n}^2\, \mathrm{d}S, \tag{21}$$

where the integration is performed over the whole surface of the system, $\overline{v} = \frac{3}{4} v_F$ is the average nucleon velocity, and

$$\dot{n}^2 = \frac{\left|\frac{\partial \mathcal{R}}{\partial t}\right|^2}{|\nabla \mathcal{R}|^2}, \quad \mathcal{R} = r - R(\theta). \tag{22}$$

Hence we get the following expressions for the dissipation tensor R_{ij}:

$$R_{i,j} = 2^{|i-j|}\pi m \rho_0 \overline{v} \int_0^\pi \frac{\left\{ R_0 \left\{ \frac{\partial \beta_1}{\partial \beta_i} Y_{10} + Y_{i0} \right\} + \frac{\partial R_0}{\partial \beta_i} S \right\}}{1 + \frac{1}{R^2(\theta)} \left\{ \frac{\partial R(\theta)}{\partial \theta} \right\}^2} \times \left\{ R_0 \left\{ \frac{\partial \beta_1}{\partial \beta_j} Y_{10} + Y_{j0} \right\} + \frac{\partial R_0}{\partial \beta_j} S \right\} R^2(\theta) \sin\theta\, \mathrm{d}\theta. \tag{23}$$

6. The Langevin term

The stochastic force $F_{\text{fluc}}(t)$ will determine fluctuations in momentum space, according to the value of the diffusion coefficient D. We assume that

$$\langle F_{\text{fluc}}(t) F_{\text{fluc}}(t+s) \rangle = D\delta(s). \tag{24}$$

The action of the stochastic force F_{fluc} may be simulated numerically by repeatedly producing a random kick δP in the collective velocity associated with the quadrupole and octupole moments. The value of δP is chosen randomly from a Gaussian distribution with mean value and variance given by

$$\overline{\delta P} = 0, \tag{25}$$

$$\overline{(\delta P)^2} = D\delta t, \tag{26}$$

where δt is the small time step between two kicks. The diffusion coefficient D can be found using the Einstein relation:

$$D = 2T\gamma, \tag{27}$$

where γ is the dissipation coefficient and T is the temperature of the system [31]. Hence the fluctuations that we are considering are induced essentially by the thermal agitation. We note that our dissipation tensor R_{ij}, introduced previously, also has nondiagonal terms. Hence, to correctly extract the dissipation coefficients, we diagonalize the dissipation tensor $R_{ij} \to \gamma_{ij}$. The tensor γ_{ij} will have only diagonal elements: γ_2 and γ_3. Now we can find D_2 and D_3 in the new coordinate system and evaluate δP_2 and δP_3, the random kicks for the new coordinates. Finally, it is possible to go back to the general coordinates β_2 and β_3, by the inverse transformation, and obtain δP_{β_2} and δP_{β_3}.

In conclusion, we essentially follow a semiclassical treatment also for the description of the dynamics of shape observables, looking, in particular, at quadrupole and octupole oscillations, which may lead to rather elongated configurations of the system under study. In this context, the fluctuations inserted in the dynamics of the collective oscillations are of a thermal nature, as discussed previously. It would be interesting to include also the contribution of quantal (zero-point) fluctuations of these surface modes, as the frequencies are of the order of the temperature [31]. This would increase the overall amplitude of surface oscillations, inducing larger fluctuations in the system configuration. For instance, the importance of zero-point fluctuations of vibrational modes of the nuclear surface hwas recently pointed out in an evaluation of fusion cross sections in heavy-ion collisions at near- and sub-barrier energies [32]. In our "exit channel" case we would expect just the opposite, that is, a larger breakup probability.

III. RESULTS

We exploit the Langevin treatment outlined in Sec. II to investigate the competition between (incomplete) fusion and binary breakup mechanisms in low-energy reactions. We consider the system $^{36}\text{Ar} + {}^{96}\text{Zr}$ at two beam energies, 9 and 16 MeV/nucleon, in the following range of impact parameters: $b = 5$–7 fm and $b = 4$–6 fm at 9 and 16 MeV/nucleon, respectively. Within this selection, according to the SMF dynamical evolution, one observes the formation of quasi-stationary elongated configurations for which fluctuations are expected to be crucial in determining the following evolution. For lower impact parameters, the conditions of the reactions are such that one always obtains incomplete fusion, while for larger impact parameters binary breakup is observed. Contour plots of the density in the reaction plane, as obtained in SMF calculations, are displayed in Figs. 1 and 2 for the two reactions.

Description of the system in terms of the global observables β_2, β_3, and ω begins at the moment when, according to the full SMF evolution, the composite system reaches a quasi-stationary shape, having dissipated almost completely the radial part of the kinetic energy deposited in the system, while the

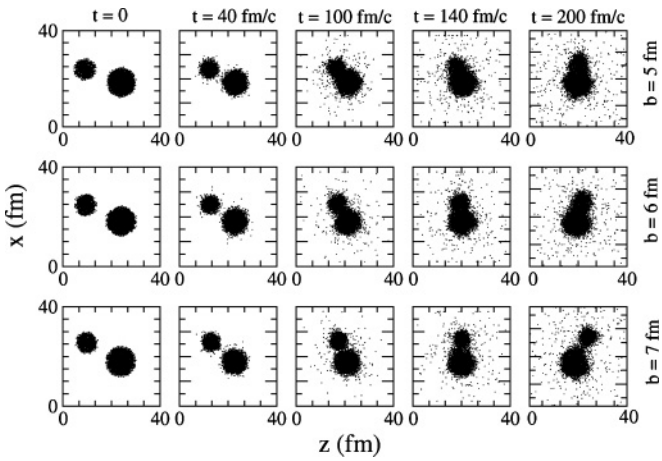

FIG. 1. Contour plots of the density projected on the reaction plane calculated with the SMF for the reaction $^{36}\mathrm{Ar} + {}^{96}\mathrm{Zr}$ at 9 MeV/nucleon, at several times (fm/c). The size of each box is 40 fm.

angular part is converted into intrinsic spin. This time instant is estimated to be around $t_{\text{freeze-out}} \approx 200$ fm/c. During the earlier dynamical evolution, pre-equilibrium nucleon emission takes place. As a consequence, the mass and charge of the system are smaller than the total mass and charge numbers, respectively. We get $A \approx 122$, $Z \approx 53$. As shown in Figs. 1 and 2, the system configuration can be suitably parametrized in terms of quadrupole and octupole moments. From this point of view, the Langevin treatment introduced previously appears to be appropriate for describing the following evolution, although the dynamical description is devolved to a few leading degrees of freedom. The initial conditions of the Langevin equation were determined running 10 SMF trajectories. The corresponding parameters are listed in Tables I and II, for a couple of events, for each considered case.

Then, within the Langevin treatment, 200 stochastic events were considered for each SMF trajectory. Fluctuations were injected each 3 fm/c.

According to the values listed in Tables I and II, we test essentially the behavior of composite systems with a variety of conditions of angular momentum, ranging from 50 to 100 $\hbar$,

TABLE I. Characteristics of the composite system, as obtained in the reaction $^{36}\mathrm{Ar} + {}^{96}\mathrm{Zr}$ at 9 MeV/nucleon at time $t_{\text{freeze-out}}$: excitation energy, intrinsic angular momentum, quadrupole moment, octupole moment and associated collective velocities. The time unit adopted to define the collective velocities is 10^{-22} s = 30 fm/c. Two events are displayed for each impact parameter. The fission probability (see text) is reported in the last column.

b (fm)	E^* (MeV)	L ($\hbar$)	β_2	β_3	$d\beta_2/dt$	$d\beta_3/dt$	P
7	225	100	1.14	−0.73	0.099	0.024	0.990
7	242	95	1.00	−0.76	0.143	−0.129	0.990
6	240	77	0.83	0.47	0.062	−0.010	0.645
6	224	84	1.01	−0.52	0.113	−0.063	0.880
5	216	64	0.58	−0.32	0.125	0.938	0.375
5	227	58	0.56	0.36	−0.004	0.005	0.145

TABLE II. Same as Table I, but for the reaction at 16 MeV/nucleon.

b (fm)	E^* (MeV)	L ($\hbar$)	β_2	β_3	$d\beta_2/dt$	$d\beta_3/dt$	P
6	279	90	0.88	0.34	0.016	0.059	1.000
6	277	97	0.88	0.44	−0.015	−0.031	1.000
5	241	73	0.37	0.15	−0.063	−0.047	0.320
5	252	77	0.63	0.40	0.136	−0.020	0.580
4	258	63	0.31	0.06	0.052	0.018	0.110
4	247	52	0.22	0.05	−0.007	0.002	0.035

and quadrupole moment β_2, from 0.2 to 1. The excitation energy is about 250 MeV, corresponding to temperatures of the order of 4 MeV. Apart from the situation observed in the case of $b = 7$ fm, $E/A = 9$ MeV/nucleon, the octupole moment β_3 always takes rather small values, of both signs, indicating that the memory of the entrance channel mass asymmetry is lost. Also, the quadrupole and octupole collective velocities are rather low and may take values of both signs, suggesting that collective motions, apart from the rotation associated with the intrinsic spin, are damped. These conditions correspond closely to quasistationary, metastable situations; that is, the system is stable against small shape fluctuations. On one hand, it may evolve radiating its excitation energy and spin and relaxing slowly toward the spherical configuration. On the other hand, if the amplitude of the kicks of the associated collective velocities is high enough, the system may overcome the fission barrier and reach configurations corresponding to surface instabilities, from which it rapidly separates into two pieces. However, one should also consider that the latter possibility is in competition with nucleon emission, which reduces the excitation energy (and the associated amplitude of thermal fluctuations), while the shape of the system is evolving. The nucleon emission rate can be evaluated according to the standard Weisskopf formalism [33]. For the situations under study, the excitation energy decreases, owing to nucleon emission, by approximately 2.5 MeV each 30 fm/c. We follow the trajectory of the system until the available excitation energy is fully dissipated.

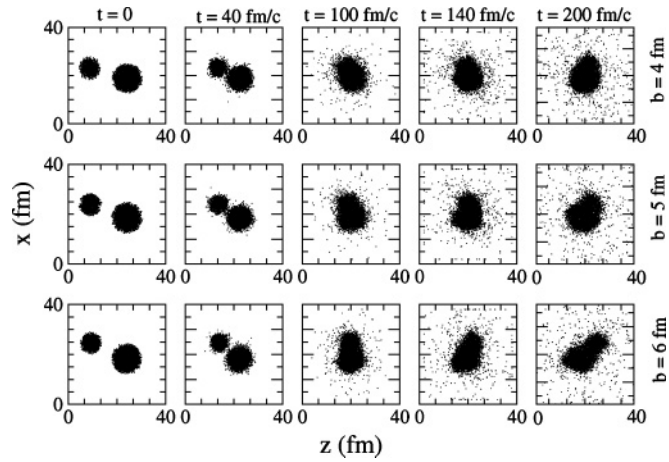

FIG. 2. The same as Fig. 1 but at 16 MeV/nucleon.

Hence, thanks to the introduction of fluctuations in the dynamical evolution, for a given impact parameter one observes a bifurcation of trajectories, leading either to compact shapes (fusion) or to elongated shapes, with large values of quadrupole and/or octupole moments, which eventually cause the breakup of the system. Actually the two possible outcomes are associated with a kind of bimodal behavior of the shape observables, related to configurations corresponding to local minima of the total (surface + Coulomb) energy. It is interesting that bimodality has recently been observed also in the context of liquid-gas phase transitions, where volume instabilities are concerned and dilute systems may either recompact to normal density or split into a huge number of small fragments [34].

A. Fission rates

In the following, we first discuss some illustrative results obtained in the case of the reaction at 16 MeV/nucleon, $b = 5$–6 fm. In Fig. 3 we present one example of trajectories corresponding to the two possible exit channels (fusion or fission), in the (β_2, β_3) plane. Because of the random kicks, starting from the same initial conditions, rather different paths are explored. It should be noted that, also in the case of trajectories leading to fusion, the final configuration is not exactly spherical, but is associated with small (not vanishing) values of the quadrupole moment. This corresponds to the stationary configuration compatible with the amount of intrinsic angular momentum present in the system. On the contrary, breakup configurations are characterized by rather large values of β_2 and/or β_3. Actually one sees an interesting correlation between the two parameters, which is represented in Fig. 4. In fact, both large quadrupole and large octupole moments are linked to breakup configurations, that correspond to tangent spheroids. Fluctuations of the octupole moment are rather large, although the majority of the events is located near $\beta_3 = 0$, corresponding to symmetric fission.

In Figs. 5 and 6 (left) the fission rate, dN/dt, as obtained for $b = 6$–7 fm at 9 MeV/nucleon and $b = 5$–6 fm at

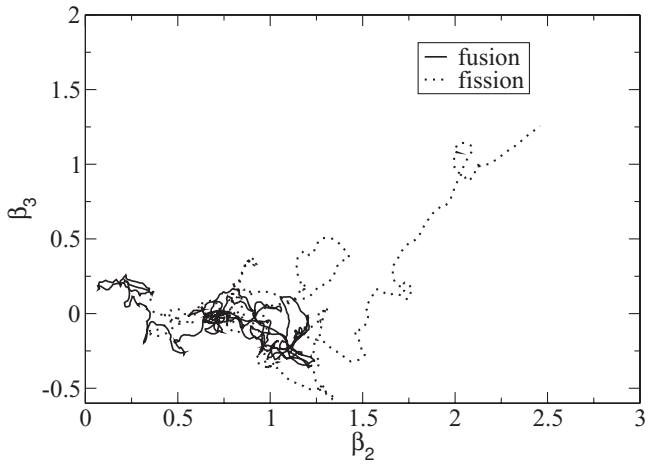

FIG. 3. One example of trajectories leading either to fusion or to breakup, in the (β_2,β_3) plane, as obtained in the reaction at 16 MeV/nucleon, $b = 5$ fm.

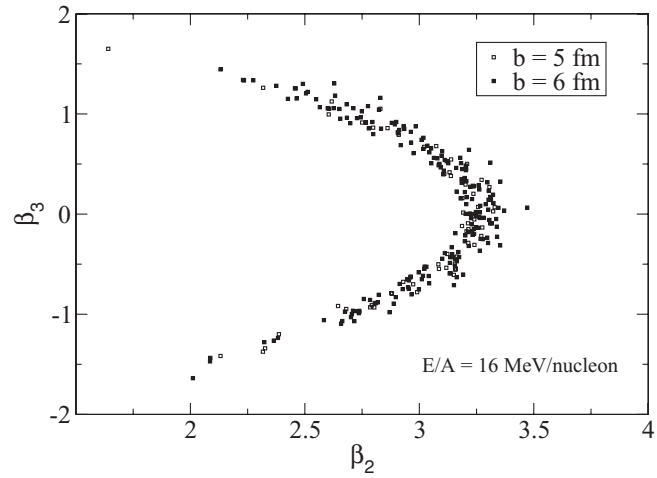

FIG. 4. Correlations between the values of quadrupole and those of octupole moments, as obtained for the breakup configurations in the case of the reaction at 16 MeV/nucleon, $b = 5$–6 fm.

16 MeV/nucleon, is displayed as a function of time for a set of 200 events in each of the cases considered. For the most peripheral impact parameters, after an initially increasing trend, related to the time interval needed to build and propagate fluctuations, we observe an almost-exponential decrease, as expected in the case of constant breakup probability $\gamma_{\rm break}$. In this case one can write $dN/dt = N_t \gamma_{\rm break}$, with $N_t = N_0 e^{-\gamma_{\rm break} t}$ and $N_0 = 200$ (the total number of events considered). This corresponds to situations where the breakup probability ($\gamma_{\rm break} \approx 0.002$ fm/c is not much affected by the competing nucleon emission. All events practically lead to fission over a time interval that is shorter than the one needed to exhaust the available excitation energy by nucleon emission. In fact, the maximum of the emission rate is observed at about 300 fm/c, and the system needs, on average, roughly 500 fm/c to reach the breakup configuration (this is actually the half-life time $\tau_{\rm break} = 1/\gamma_{\rm break}$). On the contrary, for smaller impact parameters (corresponding to lower deformation of the system and lower angular momentum), the breakup probability $\gamma_{\rm break}$ is quenched by been a factor 4 (see Figs. 5 and 6, left) and

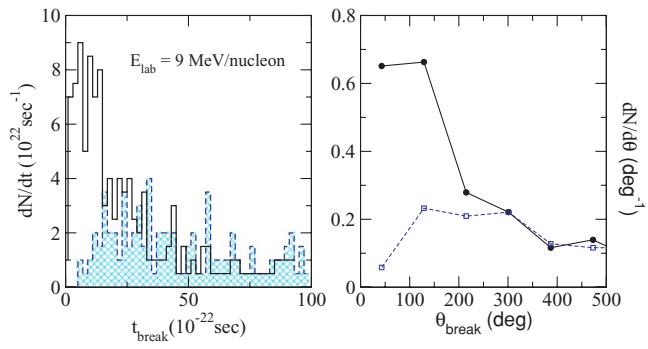

FIG. 5. (Color online) Left: Distribution of the time $t_{\rm break}$ (see text) obtained for the reaction at 9 MeV/nucleon and impact parameters $b = 7$ fm (solid histogram) and $b = 6$ fm (hatched histogram). Right: Angular distribution of the breakup direction. Solid line and circles refer to $b = 7$ fm; dashed line and open squares are for $b = 6$ fm.

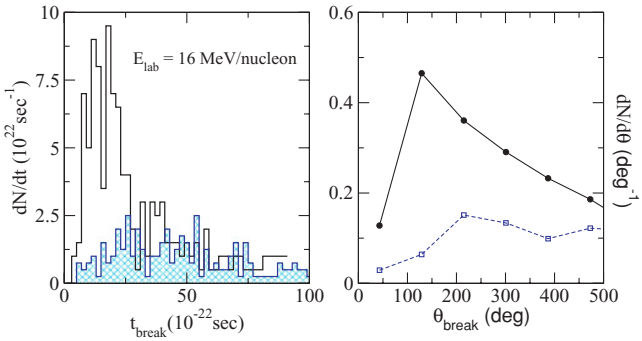

FIG. 6. (Color online) Same as Fig. 5, for the reaction at 16 MeV/nucleon and $b = 5$–6 fm.

decreases in the course of time because of nucleon emission, which reduces the excitation energy and the corresponding number of thermal fluctuations. In most cases, the excitation energy deposited in the system is dissipated before the breakup configuration can be reached. It is interesting that, even in the most favourable case, the typical durations of the process are rather long (500 fm/c), compared, for instance, to the time scales associated with the development of volume instabilities in multifragmentation processes at higher energies (about 150 fm/c). This can be explained in terms of the larger amount of excitation energy deposited in the system in the latter case (which induces fluctuations of higher amplitude and collective radial expansion) and of the shorter growth times associated with volume instabilities [20].

The corresponding fraction of events that undergo breakup, $P_{\rm break}$, is reported in Tables I and II, at the two energies and for all impact parameters considered. From the estimated breakup probabilities it is possible to construct the fusion cross section, $\sigma_f(b) = (1 - P_{\rm break})2\pi b db$, which is displayed in Fig. 7, for the two energies. We also show, for comparison, the results obtained within the SMF approach only, where, owing to the approximate treatment of fluctuations, one gets distributions

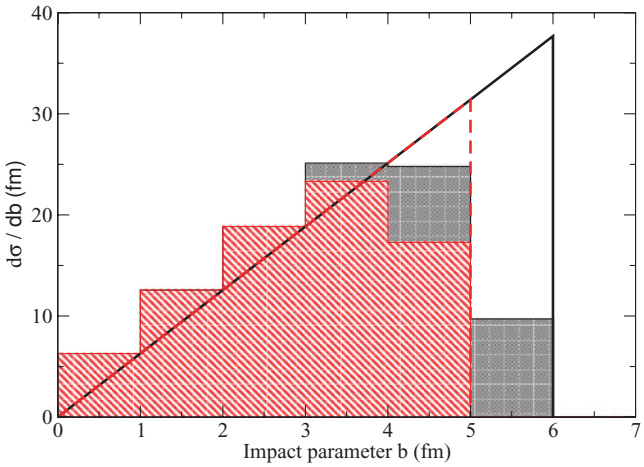

FIG. 7. (Color online) Fusion cross section, as a function of the impact parameter b, obtained in the reactions at 9 MeV/nucleon (black histogram) and 16 MeV/nucleon (gray histogram) with the Langevin treatment, Eq. (4). Lines correspond to SMF simulations at 9 MeV/nucleon (solid) and 16 MeV/nucleon (dashed).

close to a sharp cutoff (approximated by the sharp cutoff in the figure). It is interesting that, especially in the case of the reaction at 9 MeV/nucleon, the fusion cross section is reduced significantly by the introduction of fluctuations, which, in turn, help the system to overcome the fission barrier and to breakup.

B. Features of fission fragments

The time $t_{\rm break}$, needed to reach the breakup configuration, is connected to other interesting features of the reaction dynamics, depending on the various entrance-channel conditions. In fact, owing to the intrinsic spin, the system rotates while its shape evolves according to Eq. (4). As a consequence, the direction along which the system separates into pieces is strictly connected to $t_{\rm break}$. Hence the shape of the angular distribution of fission fragments can be used as a clock of the collision, from which one can extract information on the breakup probability and the underlying reaction mechanism. This is an appealing issue that can be investigated also experimentally by looking at the angular distribution of the emerging reaction products and at the possible existence of alignment effects [9,10]. In the case of a fast breakup (fast fission), the angular distribution should exhibit a peak: owing to the elongated shape of the system, the emission is not isotropic. Along the separation process, fragments acquire velocities essentially owing to the Coulomb repulsion, according to the Viola systematics, as in standard fission, but with a preferential emission axis. The distribution of the angle $\theta_{\rm break}$, corresponding to the rotation (on the plane perpendicular to the direction of the intrinsic spin of the system) until the breakup configuration is reached, is shown in Figs. 5 and 6 (right), for the two energies and two impact parameters. Obviously, the shape of this distribution depends on the fission probability, but also on the system angular velocity (which in turn depends on the intrinsic spin). In fact, in the absence of rotation (vanishing spin) the fragments would always be emitted along a fixed axis. In the case of the most peripheral events, a clear peak is observed in the distribution. On the contrary, for more central impact parameters, the half-life time is much larger and one essentially gets a flat distribution for $\theta_{\rm break}$, similarly to what is expected in the case of standard statistical fission.

C. Fast fission of projectile-like and targetlike fragments

Several shape, angular momentum, and excitation energy conditions can be observed also in the case of collisions between heavy systems, after separation into PLFs and TLFs, for one (or both) of these products. Thus it is interesting to investigate fast-fission processes of these objects, leading to ternary (or quaternary) breaking of the whole system. For instance, Fig. 8 shows density contour plots obtained in SMF simulations of semiperipheral collisions of Au + Au at 15 MeV/nucleon, for which aligned ternary and quaternary breaking has recently been observed experimentally [9]. One can see that shape configurations similar to those observed in the reactions investigated here, may appear for PLFs and TLFs. However, these fragments have a lower angular momentum (about 20–40 $\hbar$) and excitation energy (of the order of 100 MeV). The corresponding breakup probability is of the

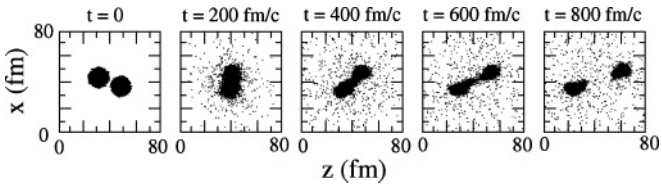

FIG. 8. Contour plots of the density projected on the reaction plane calculated with the SMF for the reaction $^{197}\mathrm{Au} + {}^{197}\mathrm{Au}$ at 15 MeV/nucleon, $b = 6$ fm, at several times (fm/c). The size of each box is 80 fm.

order of 10% and emission times are longer (≈2000 fm/c). The fast-fission mechanism could explain qualitatively some of the features observed experimentally, such as alignment effects and fragment relative velocities and charge distributions. However, a thorough analysis of the kinematical properties of the reaction products [9], as well as the rather short estimated breakup times, suggests the persistence of nonequilibrium effects in momentum space, that is, the presence of collective velocities in β_2 and/or β_3, in addition to the tangential velocity generated by the intrinsic angular momentum. Collective velocities, probably underestimated in the SMF calculations, would speed up the fragmentation process, as the system is pushed toward more exotic shapes, from which it is easier to overcome the fission barrier.

IV. CONCLUSIONS

In this article we have investigated the role of shape fluctuations in the dynamical evolution of excited systems that can be formed in semiperipheral reactions at low energies (∼20 MeV/nucleon). Quasistationary composite systems, with quadrupole and/or octupole deformation, are observed, for which shape fluctuations are essential to overcome the fission barrier and eventually break up. This analysis is performed within a hybrid treatment that couples study of the early stage of the dynamics, devolved to a microscopic stochastic transport approach, up to the formation of primary excited sources, to a full Langevin description of the leading degrees of freedom of these objects: quadrupole and octupole moments and angular velocity. For temperature, shape, and angular momentum conditions obtained in semi-peripheral reactions, typical time scales of the break-up process are of the order of 500 fm/c. The fission fragments are emitted along a preferential direction, which corresponds to the maximum elongation axis. Because of angular momentum effects, this direction may rotate while the shape of the system is evolving toward breakup configurations. Hence a careful analysis of the angular distribution of the reaction products may give relevant information on fission probabilities and the time scales involved, which in turn are closely linked to the mean-field dynamics and the properties of the nuclear interaction (range, surface energy, two-body correlations). From this study it is clear that a good treatment of mean-field fluctuations is a crucial point in the characterization of dissipative reactions. The model employed here provides a suitable description of surface modes, parametrized in terms of quadrupole and octupole oscillations, but it could miss some nonequilibrium effects that can help the system to break up. In fact, collective velocities related to shape observables are likely underestimated in the SMF approach [35] and the role of multipolarities higher than octupole is neglected in the Langevin treatment.

Moreover, we reiterate the expected relevance in our separation dynamics of the interplay between quantum zero-point and thermal fluctuations; see the end of Sec. II. A consistent treatment of both will certainly reduce the breakup time, in the direction of the alignment signal observed in Ref. [9] in ternary and quaternary events.

A fully microscopic description of the whole process would be highly desirable, although it is far from being trivial. Some attempts are represented by improved quantum molecular dynamics calculations [19]. Stochastic extensions of time-dependent Hartree-Fock calculations should also provide a valuable tool to characterize reaction mechanisms in low-energy collisions [36]. Work in this direction is in progress.

[1] P. Lautesse *et al.*, Eur. Phys. J. A **27**, 349 (2006).
[2] T. C. Awes *et al.*, Phys. Rev. Lett. **52**, 251 (1984).
[3] V. Penumetcha *et al.*, Phys. Rev. C **42**, 1489 (1990).
[4] M. Colonna, M. Di Toro, and A. Guarnera, Nucl. Phys. A **589**, 160 (1995).
[5] F. Amorini *et al.*, Phys. Rev. Lett. **102**, 112701 (2009).
[6] V. Baran, M. Colonna, V. Greco, and M. Di Toro, Phys. Rep. **410**, 335 (2005).
[7] P. Glassel, D. v. Harrach, H. J. Specht, and L. Grodzins, Z. Phys. A **310**, 189 (1983).
[8] A. A. Stefanini *et al.*, Z. Phys. A **351**, 167 (1995).
[9] I. Skwira-Chalot *et al.*, Phys. Rev. Lett. **101**, 262701 (2008); J. Wilczynski *et al.*, Phys. Rev. C **81**, 024605 (2010).
[10] De Filippo *et al.*, Phys. Rev. C **71**, 044602 (2005).
[11] D. Boilley, E. Suraud, Y. Abe, and S. Ayik, Nucl. Phys. A **556**, 67 (1993).
[12] S. Ayik and C. Gregoire, Phys. Lett. B **212**, 269 (1988), and refs. therein.
[13] J. Rizzo, P. Chomaz, and M. Colonna, Nucl. Phys. A **806**, 40 (2008), and refs. therein.
[14] P. Danielewicz, R. Lacey, and W. G. Lynch, Science **298**, 1592 (2002).
[15] A. Guarnera, M. Colonna, and Ph. Chomaz, Phys. Lett. B **373**, 267 (1996).
[16] M. Colonna *et al.*, Nucl. Phys. A **642**, 449 (1998).
[17] V. Baran *et al.*, Nucl. Phys. A **600**, 111 (1996).
[18] M. Papa *et al.*, Phys. Rev. C **68**, 034606 (2003); **72**, 064608 (2005).
[19] Tian Jun-Long *et al.*, Chinese Phys. C **33**, 109 (2009).
[20] P. Chomaz, M. Colonna, and J. Randrup, Phys. Rep. **389**, 263 (2004).
[21] S. Ayik, M. Colonna, and P. Chomaz, Phys. Lett. B **353**, 417 (1995).
[22] W. Wen, P. C. Huu-Tai, D. Lacroix *et al.*, Nucl. Phys. A **637**, 15 (1998).

[23] J. Błocki, Y. Boneh, J. R. Nix, J. Randrup, M. Robel, A. J. Sierk, and W. J. Świątecki, Ann. Phys. **113**, 330 (1978).
[24] J. R. Nix, Ann. Phys. **41**, 52 (1967).
[25] H. J. Krappe, J. R. Nix, and A. J. Sierk, Phys. Rev. C **20**, 992 (1979).
[26] P. Möller and J. R. Nix, Nucl. Phys. A **361**, 117 (1981).
[27] P. Möller and J. R. Nix, At. Data Nucl. Data Tables **39**, 213 (1988).
[28] A. J. Sierk, Phys. Rev. C **33**, 2039 (1986).
[29] K. T. R. Davies and J. R. Nix, Phys. Rev. C **14**, 1977 (1976).
[30] W. D. Myers, Nucl. Phys. A **145**, 387 (1970).
[31] L. D. Landau and E. M. Lifshitz, *Statistical Physics* Part 1. Vol. 5 (3rd ed.) (Butterworth-Heinemann, 1980).
[32] S. Ayik, B. Yilmaz, and D. Lacroix, Phys. Rev. C **81**, 034605 (2010).
[33] G. F. Bertsch, P. G. Reinhard, and E. Suraud, Phys. Rev. C **53**, 1440 (1996).
[34] E. Bonnet *et al.*, Phys. Rev. Lett. **103**, 072701 (2009).
[35] M. Colonna *et al.*, Nucl. Phys. A **742**, 337 (2004).
[36] K. Washiyama, S. Ayik, and D. Lacroix, Phys. Rev. C **80**, 031602(R) (2009).